



ISSN: 0095-8972 (Print) 1029-0389 (Online) Journal homepage: <http://www.tandfonline.com/loi/gcoo20>


Catalytic oxygenation of various monophenols by copper(I) complexes with bis(pyrazolyl)methane ligands: differences in reactivity

Jessica Nadine Hamann, Rebecca Schneider & Felix Tuczek

To cite this article: Jessica Nadine Hamann, Rebecca Schneider & Felix Tuczek (2015) Catalytic oxygenation of various monophenols by copper(I) complexes with bis(pyrazolyl)methane ligands: differences in reactivity, *Journal of Coordination Chemistry*, 68:17-18, 3259-3271, DOI: 10.1080/00958972.2015.1074191

To link to this article: <http://dx.doi.org/10.1080/00958972.2015.1074191>




View supplementary material 



Accepted author version posted online: 24 Jul 2015.
Published online: 13 Aug 2015.



Submit your article to this journal 



Article views: 79



View related articles 



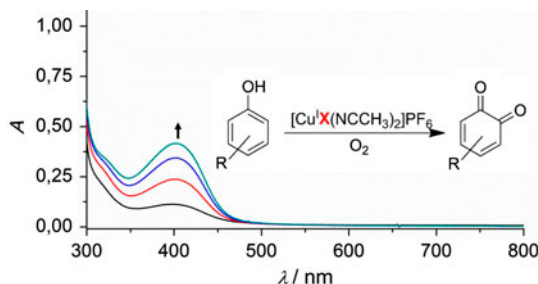
View Crossmark data 

Catalytic oxygenation of various monophenols by copper(I) complexes with bis(pyrazolyl)methane ligands: differences in reactivity

JESSICA NADINE HAMANN, REBECCA SCHNEIDER and FELIX TUCZEK*

Institute of Inorganic Chemistry, Christian-Albrechts-University, Kiel, Germany

(Received 6 May 2015; accepted 14 July 2015)



Three new mononuclear copper(I) complexes supported by the symmetric ligands 1,1'-methylenebis-1*H*-pyrazole (**BPM**), 1,1'-methylenebis(3-methyl-1*H*-pyrazole) (**mBPM**), and 1,1'-methylenebis(3,5-di-methyl-1*H*-pyrazole) (**dmBPM**) were synthesized as catalytic model systems of tyrosinase. The influence of various functional groups on the catalytic conversion of monophenols is investigated and the formation of the corresponding *ortho*-quinones is monitored using UV/vis and NMR spectroscopy. Comparison of various monophenols reveals the differences in reactivity which are analyzed and interpreted based on key intermediates of the mechanistic cycle.

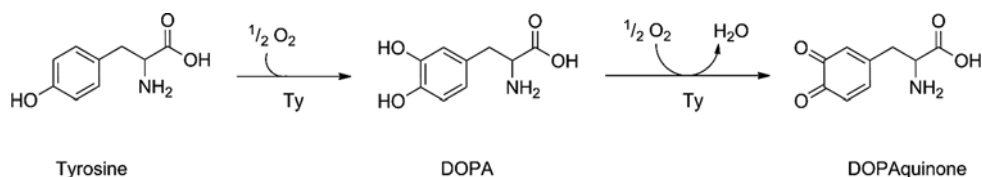
Keywords: Type 3 copper enzymes; Tyrosinase; Model systems; *Ortho*-hydroxylation; Pyrazole

1. Introduction

The copper containing enzyme tyrosinase (Ty) catalyzes the monooxygenation of the amino acid tyrosine which is first hydroxylated to *L*-DOPA (*L*-dihydroxyphenylalanine; monophenolase activity) that subsequently is converted in a two-electron oxidation to dopaquinone (diphenolase activity, scheme 1). Dopaquinone acts as precursor for the biosynthesis of melanin, a pigment that is involved in all biological browning processes [1–4].

The first X-ray crystal structure of tyrosinase was obtained from the bacterium *Streptomyces castaneoglobisporus* by Matoba and coworkers in 2006. During the last years,

*Corresponding author. Email: ftuczek@ac.uni-kiel.de



Scheme 1. Formation of dopaquinone, starting from tyrosine via DOPA, catalyzed by tyrosinase.

more crystal structures were determined [5–8]. All of them show that the active site of tyrosinase contains a binuclear type 3 copper center whereby three histidine residues surround each copper ion (figure 1) [9]. The two other proteins having type 3 copper active sites are hemocyanin (Hc) and catechol oxidase (CO). Hemocyanin mediates the oxygen transport in arthropods and molluscs, whereas catechol oxidases are responsible for the two-electron oxidation of catechols to the corresponding *ortho*-quinones [10]. All type 3 copper proteins in their *oxy* form bind dioxygen as peroxide in a typical side-on bridging geometry ($\mu\text{-}\eta^2\text{:}\eta^2$) whereby both copper ions oxidized from Cu^{I} to Cu^{II} [9]. The $\text{Cu}(\text{II})_2$ side-on peroxo core shows characteristic properties in the optical and vibrational spectra. In the UV/vis absorption spectrum, an intense band of the peroxide $\rightarrow \text{Cu}$ CT transition is observable at ~ 350 nm, and the Raman spectrum shows an O–O stretching vibration at ~ 750 cm^{-1} [2].

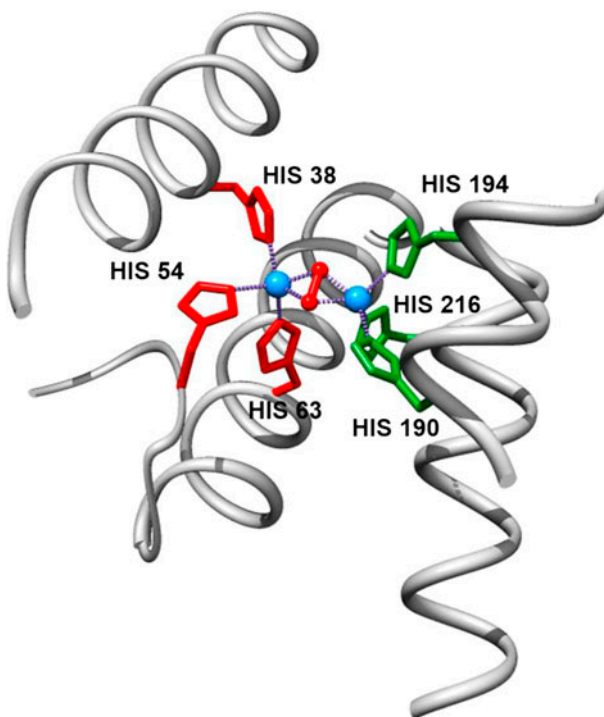


Figure 1. Active site of tyrosinase isolated from *S. castaneoglobisporus* [5].

During the last 30 years, many copper complexes have been investigated as small-molecule models of tyrosinase. These systems are able to hydroxylate (i) an aromatic part of the ligand framework [11–17] or (ii) external phenolic substrates [18–25] whereby the latter reactivity can be stoichiometric or catalytic. The first catalytic model system of tyrosinase was described by Réglier and coworkers in 1990 [19]. The copper(I) complex of their BiPh (impy)₂ ligand was able to convert the monophenol 2,4-di-*tert*-butyl-phenol (2,4-DTBP-H) to the corresponding 3,5-di-*tert*-butyl-*ortho*-quinone (3,5-DTBQ) in 16 turnovers. Another system has been reported by Casella and coworkers in 1991 which exhibits stoichiometric as well as catalytic monooxygenation of external phenols [18]. The first model system of tyrosinase based on a mononucleating ligand has been described by our group in 2010. The ligand **L_{py}1** contains a pyridine ring and a *tert*-butyl-terminated imine function. The Cu**L_{py}1** complex is able to convert the substrate 2,4-DTBP-H to the corresponding 3,5-DTBQ with a *turnover number* (TON) of 22 [20, 24]. In 2013, Herres-Pawlis and coworkers established a model system of tyrosinase that is based on the tridentate ligand HC (3-*t*BuPz)₂(Py) which is composed of two *tert*-butyl-substituted pyrazoles and a pyridine moiety. This system was the first one which both forms a room temperature stable peroxo intermediate and shows catalytic activity regarding the hydroxylation of monophenols [22]. In recent years, further small-molecule models of tyrosinase were developed by our group in which the pyridine ring of **L_{py}1** was replaced by a benzimidazole and a pyrazole ring, leading to the bidentate ligands **L_{bzm}1**, **L_{hpy}1**, and **L_{hpy}2**, respectively. The corresponding copper complexes were found to convert DTBP-H to DTBQ with TONs of 31, 29, and 23, respectively [23, 24].

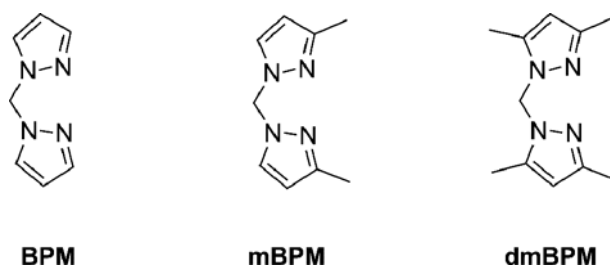
To obtain further insight into the structural and electronic influences of the ligands on the catalytic activity of the corresponding copper complexes, we now set out to replace the imine function of the bidentate **L_x** ligands by a second heterocycle, generating symmetric ligands. Replacement of the imine function in the **L_{py}1** ligand by pyridine led to the dipyridylmethane **L3**. The Cu**L3** complex, however, was found to be inactive with respect to the catalytic oxygenation of DTBP-H [20]. In an effort to replace the imine functions of the **L_{hpy}1** and **L_{hpy}2** ligands by a second pyrazole group, we now investigate copper complexes supported by 1,1'-methylenebis-1*H*-pyrazole (**BPM**), 1,1'-methylenebis(3-methyl-1*H*-pyrazole) (**mBPM**), and 1,1'-methylenebis(3,5-dimethyl-1*H*-pyrazole) (**dmBPM**, scheme 2). Bis(pyrazolyl)methane-based ligands have been employed for model systems of tyrosinase before [22, 26].

Herein the catalytic activity of Cu(I) complexes of **BPM**, **mBPM**, and **dmBPM** regarding the *ortho*-hydroxylation of monophenols is investigated. Besides the standard substrate 2,4-DTBP-H, a range of other monophenols is studied as well (scheme 3). The different reactivities are analyzed and interpreted on the basis of key intermediates of the mechanistic cycle.

2. Results and discussion

2.1. Syntheses of the ligands and the corresponding copper(I) complexes

The symmetric pyrazole ligands **BPM**, **mBPM**, and **dmBPM** were prepared in one-step syntheses, starting from the corresponding pyrazoles which were coupled with dibromomethane in DMSO [27]. The corresponding copper(I) complexes were prepared from tetrakis(acetonitrile)copper(I) hexafluorophosphate under anaerobic conditions (scheme 4).



Scheme 2. Synthesized symmetric N-donor ligands for further copper(I) model systems of tyrosinase.

2.2. Investigation of catalytic activity

The catalytic activity of the symmetric model systems can be monitored by *in situ* UV/vis spectroscopy because *ortho*-quinones show an intense absorption at 390–450 nm, having ϵ values from 1100 to 1800 $\text{M}^{-1} \text{cm}^{-1}$ [28]. Catalytic oxygenation reactions were performed at room temperature. To this end, a 500 μM solution of the respective copper(I) complex in dichloromethane was prepared and 50 eq. of the respective monophenol (scheme 3) and 100 eq. of triethylamine were added. Subsequent oxygenation at ambient temperature resulted in the formation of *ortho*-quinones, as indicated by absorption bands at 390–450 nm. The yield of formed *ortho*-quinone was determined on the basis of known extinction coefficients [28–31].

2.2.1. Catalytic monooxygenation of 2,4-DTBP-H. $[\text{Cu}^{\text{I}}\text{BPM}(\text{NCCH}_3)_2]\text{PF}_6$ catalyzes the formation of 3,5-DTBQ, starting from 2,4-DTBP-H. Figure 2 shows the UV/vis spectra of the oxygenation of 2,4-DTBP-H with $[\text{Cu}^{\text{I}}\text{BPM}(\text{NCCH}_3)_2]\text{PF}_6$ in dichloromethane

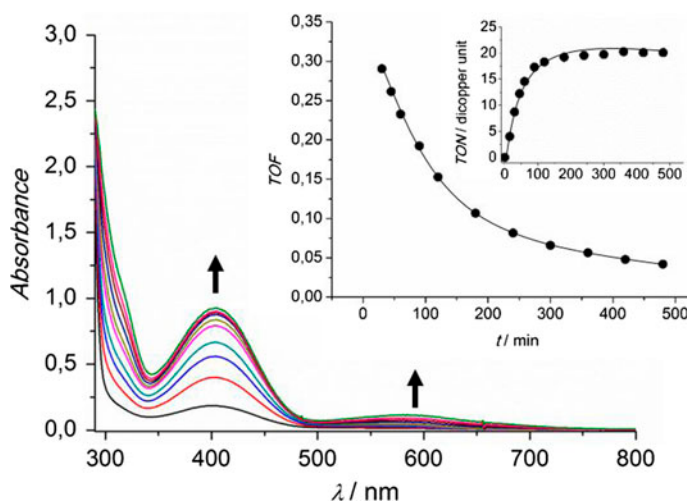
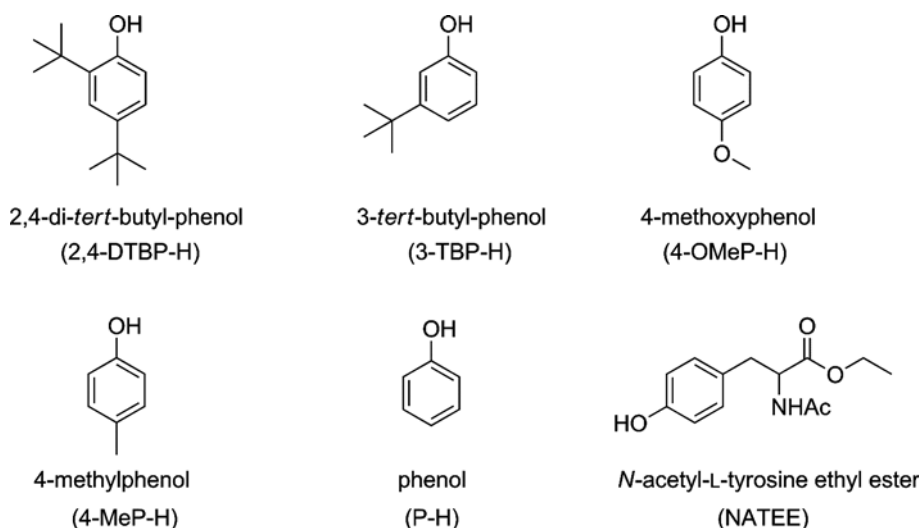


Figure 2. UV/vis spectra of a 500 μM solution of $[\text{Cu}^{\text{I}}\text{BPM}(\text{NCCH}_3)_2]\text{PF}_6$ in CH_2Cl_2 after addition of 50 eq. 2,4-DTBP-H, 100 eq. NEt_3 and oxygenation between 15 min and 6 h; $l = 1$ mm. Inset: TON and TOF vs. reaction time.



Scheme 3. Set of monophenols used as external substrates in the catalytic oxygenation reactions.

during the first 6 h. The formation of this product is indicated by an absorption at 407 nm [20, 23, 24]. Oxygenation of DTBP-H occurs rapidly during the first 90 min of reaction and then slows, leading to a final TON of 21 after 8 h of reaction (figure 2, inset).

To further prove the formation of the 3,5-DTBQ during oxygenation, NMR spectroscopy was used (figure 3). After 1 h of oxygenation, the solution was quenched with hydrochloric

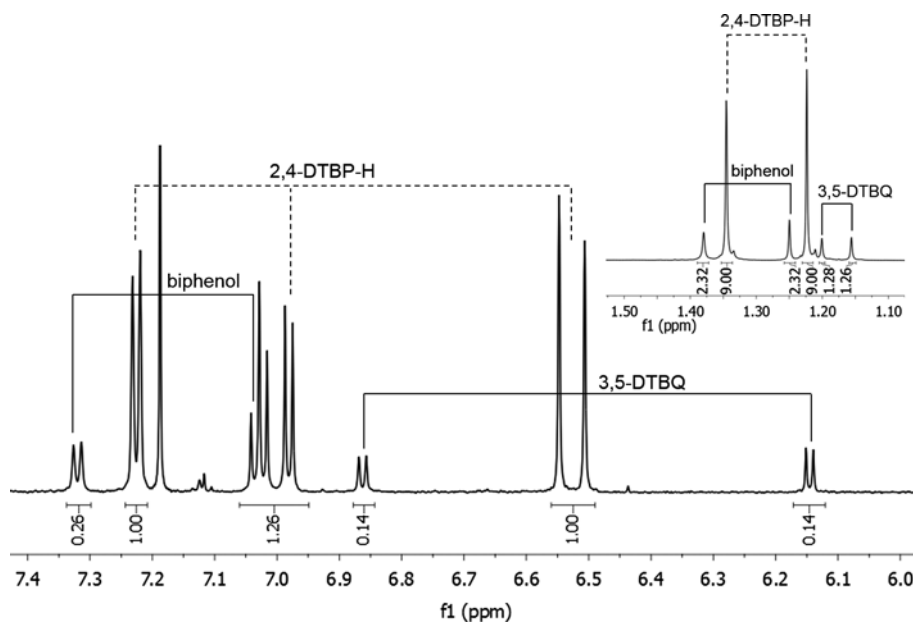
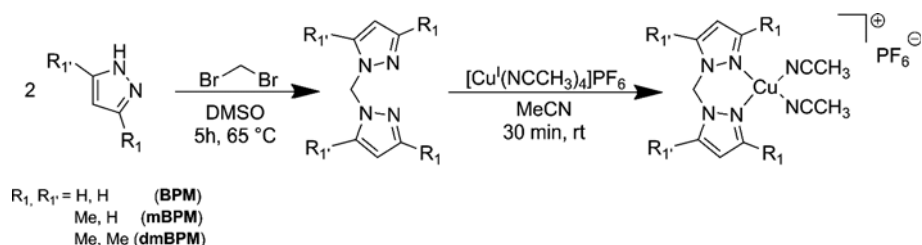


Figure 3. ^1H NMR spectrum of the oxygenation solution after quenching with HCl, measured in CDCl_3 .



Scheme 4. Synthesis overview of the symmetric ligands and their copper(I) complexes.

acid followed by several extractions with dichloromethane to remove the copper ions. In agreement with previous studies, the resulting NMR spectra revealed signals from the formed 3,5-DTBQ, the used substrate 2,4-DTBP-H, and the C–C coupling byproduct 3,3',5,5'-tetra-*tert*-butyl-2,2'-biphenol (figure 3, inset). The signals of the three compounds 2,4-DTBP-H, 3,5-DTBQ and the biphenol are present in a ratio of 60 : 14 : 26. The yield of 14% 3,5-DTBQ is in agreement with the calculated TON of 14 after 1 h of oxygenation.

Analogous experiments were performed with the other systems. Compared with $[\text{Cu}^{\text{I}}\text{mBPM}(\text{NCCH}_3)_2]\text{PF}_6$ and $[\text{Cu}^{\text{I}}\text{dmBPM}(\text{NCCH}_3)_2]\text{PF}_6$, the unsubstituted **BPM** complex shows the highest catalytic activity regarding the formation of 3,5-DTBQ (TON = 21) after 8 h of oxygenation, closely followed by the methyl-substituted **mBPM** complex (TON = 19, table 1). Using the dimethyl-substituted counterpart $[\text{Cu}^{\text{I}}\text{dmBPM}(\text{NCCH}_3)_2]\text{PF}_6$ as catalyst a TON of 11 was found (figure S1, see online supplemental material at <http://dx.doi.org/10.1080/00958972.2015.1074191>). We attribute this decrease in catalytic activity to an increasing steric demand of the **dmBPM** moiety, stabilizing the peroxo intermediate. Moreover, coordination of the substrate gets sterically hindered. Both effects lower the reaction rate with external phenols [23]. In line with these considerations, we anticipated that the least reactive **dmBPM**-based system would form the most stable peroxo intermediate, whereas the stability of the peroxo intermediate would be decreased for the more reactive **mBPM** and **BPM** systems. In fact, the peroxo species could be spectroscopically identified for the $[\text{Cu}^{\text{I}}\text{dmBPM}(\text{NCCH}_3)_2]\text{PF}_6$ complex (figure S2), whereas for the other two systems this was not possible. The absorption bands at ~350 and 550 nm increasing in

Table 1. Overview of the investigated model systems and substrates in the catalytic reactions; ϵ values relating to the formed *ortho*-quinones. Listed are the final TON after the appropriate time and TOF @ 15 min s⁻¹.

	BPM		mBPM		dmBPM	
	TON	TOF	TON	TOF	TON	TOF
2,4-DTBP-H $\epsilon = 1830 \text{ M}^{-1} \text{ cm}^{-1}$	21 (8 h)	0.27	19 (8 h)	0.24	11 (8 h)	0.22
3-TBP-H $\epsilon = 1150 \text{ M}^{-1} \text{ cm}^{-1}$	17 (8 h)	0.34	15 (8 h)	0.27	9 (8 h)	0.24
4-OMeP-H $\epsilon = 1700 \text{ M}^{-1} \text{ cm}^{-1}$	10 (1 h)	0.51	10 (1 h)	0.48	5 (1 h)	0.26
4-MeP-H $\epsilon = 1400 \text{ M}^{-1} \text{ cm}^{-1}$	14 (6 h)	0.11	12 (6 h)	0.03	10 (6 h)	0.005
P-H $\epsilon = 1417 \text{ M}^{-1} \text{ cm}^{-1}$	9 (6 h)	0.16	9 (6 h)	0.13	9 (6 h)	0.11
NATEE $\epsilon = 1180 \text{ M}^{-1} \text{ cm}^{-1}$	18 (2 h)	0.26	15 (2 h)	0.19	11 (2 h)	0.12

intensity upon oxygenation are assigned to peroxide \rightarrow copper charge transfer transitions [32]. TD-DFT calculations show agreement between the theoretical and the measured spectrum (inset figure S2).

2.2.2. Catalytic monooxygenation of other substrates. Besides 2,4-DTBP-H, five other monophenols were investigated regarding their catalytic conversion to the respective *ortho*-quinones; i.e. 4-methoxyphenol (4-OMeP-H), 3-*tert*-butyl-phenol (3-TBP-H), 4-methylphenol (4-MeP-H), the native substrate N-acetyl-L-tyrosine ethyl ester (NATEE), and unsubstituted phenol (P-H). The observed TONs and TOFs are collected in table 1 and shown pictorially in figure 4. Evidently, all of these monophenols give lower TONs than the “standard substrate” 2,4-DTBP-H. With the **BPM** system, the TON achieved for the latter substrate is more than twice as large as for the least effect substrate, P-H (TON = 9); for the **mBPM** and **dmBPM** systems, the differences are less pronounced. Regarding TOF, on the other hand, the substrate 2,4-DTBP-H only has an intermediate position. The reason for this observation is the fact that this substrate, albeit electronically activated by the *tert*-butyl groups in *ortho* and *para* position, is sterically hindered.

The second highest TON of all substrates is achieved with the substrate 3-TBP-H (TON = 17 with **BPM**). The formation of 4-*tert*-butyl-*ortho*-quinone was observed by an increasing absorption band with a maximum at 402 nm in the UV/vis spectra (figure S3). In comparison with the substrate 2,4-DTBP-H, the lack of electron-donating *tert*-butyl substituents in *ortho* and *para* positions leads to a smaller activation of 3-TBP-H toward electrophilic substitution; it is not sterically hindered.

Catalytic conversion of unsubstituted phenol (P-H) to the *ortho*-benzoquinone occurs slowly, reaching saturation after 6 h. In agreement with the complete lack of activating substituents, this is the slowest of all substrates. A characteristic absorption band at 398 nm indicates the *ortho*-hydroxylation and two-electron oxidation of phenol with a TON of 9 (figure S4).

Of particular interest with regard to biomimetic activity of our catalytic model systems is the native substrate NATEE, which was also investigated concerning the formation of the

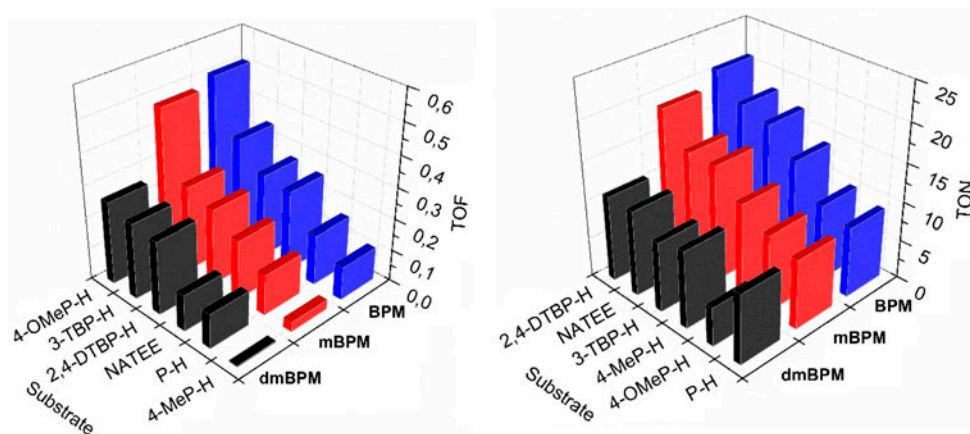
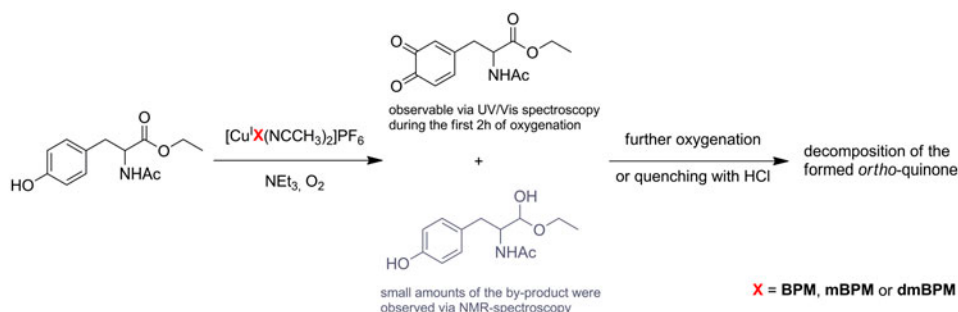


Figure 4. Comparison of the results using various substrates in the oxygenation with pyrazole model systems, left: determined TOFs at 15 min s⁻¹; right: determined TONs.



Scheme 5. Reaction behavior using the native substrate NATEE in the oxygenation.

corresponding dopaquinone derivative [33]. Using NATEE in catalytic runs with $[\text{Cu}^{\text{I}}\text{BPM}(\text{NCCH}_3)_2]\text{PF}_6$, rapid formation of the quinone is observed during the first 2 h of oxygenation. As for the other substrates, the **BPM** system shows the highest activity (TON = 18). However, after 2 h the formed quinone decomposes which is apparent in the UV/vis spectra by a shift of the absorption band from 400 to 370 nm, accompanied by an intensity decrease (figures S5 and S6). Workup of the oxygenated solution followed by NMR analysis allowed identification of the unoxygenated substrate NATEE as main product and small amounts of a byproduct which could be identified as the hemiacetal derived from reduction of the ester group (figure S7). Unfortunately, the formed dopaquinone decomposed upon quenching with aqueous hydrochloric acid, which is necessary to separate and isolate the organic compounds. A subsequently measured UV/vis spectrum exhibited no absorption at 400 nm or lower wavelength. Instability toward water probably also explains the intensity decrease in the absorption band of the quinone product in the reaction mixture after 2 h (see above; scheme 5). Nevertheless, the oxygenated product could be investigated using

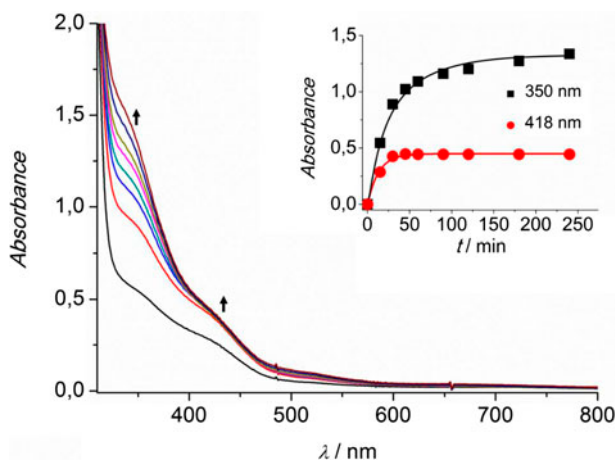
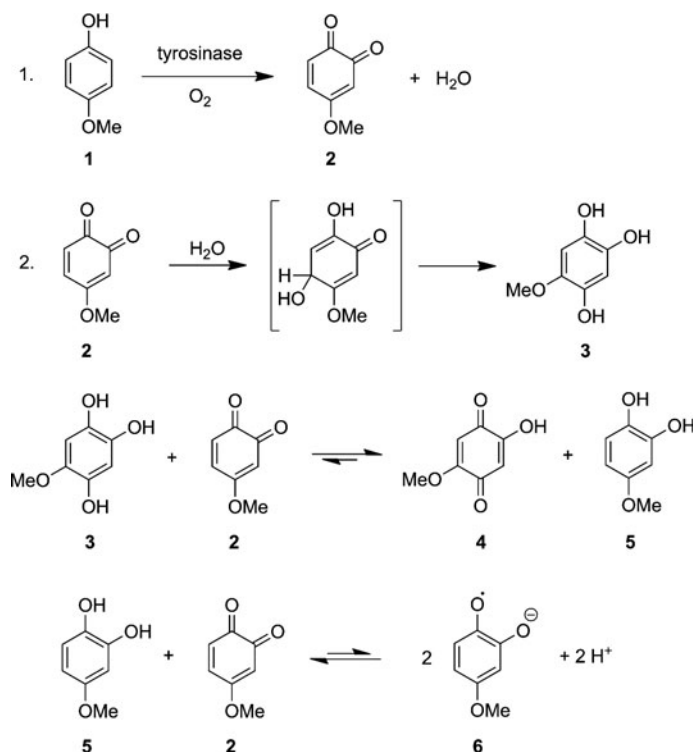


Figure 5. UV/vis spectra of the oxygenation of 4-OMeP-H with $[\text{Cu}^{\text{I}}\text{BPM}(\text{NCCH}_3)_2]\text{PF}_6$ for 4 h; after 1 h the absorption at 418 nm saturates whereas the second band at 350 nm further increases in intensity. Inset: Absorbance values vs. time; $l = 1$ mm.

mass spectrometry and a peak with low intensity could be identified at $m/z = 268.1$ which was assigned to the corresponding catechol of NATEE (ESI).

The monophenol 4-OMeP-H is the fastest of all substrates. Based on the time evolution of the absorbance at 418 nm, a TOF of 0.51 s^{-1} is achieved for the **BPM** system after the first 15 min. Saturation starts after 45 min and is complete after 60 min, leading to a TON of only 10 (figure 5). The high reaction rate is due to the strong electron-donating effect of the *para*-methoxy group, facilitating electrophilic attack by the Cu_2O_2 moiety on the arene ring in *ortho*-position to the phenolic OH group [22]. After saturation of the quinone band at 418 nm, a second band at 350 nm continues to grow in intensity (figure 5, inset). The oxygenation of 4-OMeP-H catalyzed by tyrosinase has been investigated by Riley *et al.* [34]. According to this study, the formed *ortho*-quinone product **2** is converted to the trihydroxyanisole **3** (scheme 6) [34]. Subsequently, this intermediate reacts with the *ortho*-quinone **2** to the corresponding *para*-quinone **4** and the catechol derivative **5** (scheme 6). By comproportionation of **2** and **5** semiquinone **6** is formed. While the latter product may be associated with the characteristic absorption band at 350 nm (figure 5) [35], an NMR spectrum measured after workup of the oxygenation solution showed the signals of *para*-quinone **4** besides unoxygenated 4-OMeP-H (ESI).

Anomalous behavior was also exhibited by the substrate 4-methylphenol (4-MeP-H) when subjected to oxygenation reactions (figure S9). Although the methyl group in *para* position should activate this monophenol toward hydroxylation, it shows the lowest TOF of



Scheme 6. Postulated mechanism for the reaction of 4-methoxyphenol with tyrosinase and O_2 after Riley *et al.* [34].

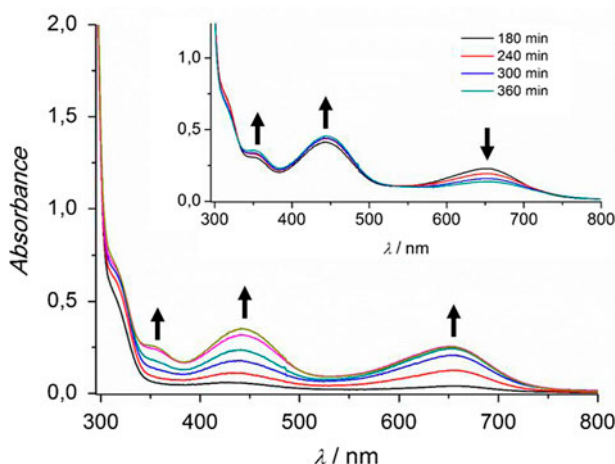


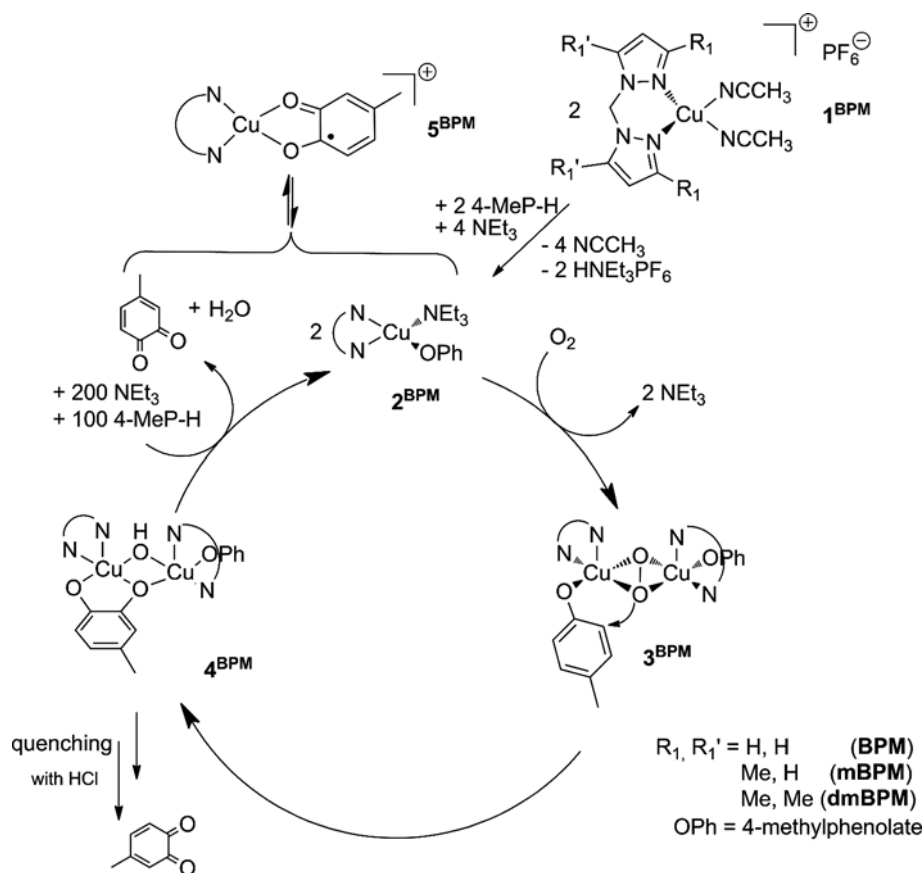
Figure 6. UV/vis spectra of the oxygenation of 4-MeP-H with $[\text{Cu}^{\text{I}}\text{BPM}(\text{NCCH}_3)_2]\text{PF}_6$ during the first 2 h. Inset: UV/vis spectra of the oxygenation for further 4 h, the intense band at 655 nm decreases; $l = 1$ mm.

all investigated substrates with 0.11 s^{-1} (**BPM** system). Based on an absorption band at 445 nm, increasing intensity during the first 6 h of oxygenation, catalytic conversion to the corresponding quinone does occur (TON = 14, figure 6). However, during oxygenation a second intense absorption emerges at 655 nm, the intensity of which decreases after 2 h (figure 6, inset) and completely disappears after 24 h (figure S10). This behavior of 4-methylphenol in oxygenation reactions is known in the literature as well and has been explained by Meyer *et al.* [36]. In phenol oxygenation reactions mediated by ruthenium oxo complexes, these authors identified a ruthenium quinone complex as an intermediate which has an absorption at 655 nm [36]. In the course of the reaction, this species disappears due to hydrolysis. We suppose that in our system a copper semiquinone complex is formed in a side reaction. Copper(II)-semiquinone derivatives have intense LMCT bands at 580–655 nm [37]. In addition, a characteristic absorption at 350 nm is observed which can be assigned to a π -system transition of free semiquinone (figure 6) [35, 37]. In the further course of the oxygenation reaction, water is formed and the copper(II) semiquinone complex is hydrolyzed. The appearance and disappearance of this intermediate is also apparent from color changes of the reaction mixture. Upon exposure to dioxygen, the color of the initially pale yellow solution changes rapidly to a light green. During further oxygenation, the light green solution becomes dark bluish green and after 24 h, the color changes to red brown.

Within our proposed mechanistic scheme [20, 23–25], formation of the Cu(II) semiquinone complex can be attributed to reaction of the primary *ortho*-quinone product with the copper(I) complex $\mathbf{2}^{\text{BPM}}$, leading to intermediate $\mathbf{5}^{\text{BPM}}$ (scheme 7). This reduces the concentration of the catalyst and explains the low reaction rate observed for this activated substrate.

3. Summary and conclusion

Three new mononuclear copper(I) complexes supported by symmetric pyrazole ligands have been synthesized and investigated as model systems of the enzyme tyrosinase which



Scheme 7. Proposed catalytic cycle for pyrazole-based symmetric systems in analogy to our previous model systems. For the last step, a competition reaction occurs, forming a Cu(II) semiquinone complex **5^{BPM}**. This reduces the amount of catalyst, lowering the reaction rate.

mediates the *ortho*-hydroxylation of external substrates. Importantly, the three **BPM** systems have catalytic activities toward the substrate DTBP-H that are comparable to those observed earlier with catalysts supported by ligands with imine groups [20, 23–25]. This is in stark contrast to the copper dipyridylmethane complex which was found to be catalytically inactive [20]. Among the copper complexes supported by bis(pyrazolyl)methane ligands, the unsubstituted **BPM** system was more reactive than its **mBPM** and the **dmBPM** derivatives. The differences between the **BPM** and **mBPM** system induced by the monosubstitution of the pyrazole are, however, small. On the other hand, the 3,5-dimethyl substitution in the **dmBPM** system leads to considerably lower catalytic activity. Presumably, this is due to the fact that the peroxo intermediate is more stable. Moreover, the increased steric hindrance induced by the methyl groups hinders coordination of the substrate to the peroxo intermediate, further lowering the reaction rate [23].

Various monophenols were subjected to catalytic oxygenations, monitored by UV/vis spectroscopy. Quite expectedly, the electron-rich phenols 2,4-DTBP-H and 3-TBP-H led to high yields of quinone. Whereas 2,4-DTBP-H turned out to be the best monophenol for our

catalytic investigations regarding the yield of quinone, the highest reaction rate was obtained with 4-methoxyphenol. However, the TON obtained with this substrate was found to be lowered due to secondary reactions of the primary reaction product. Catalytic monooxygenation of the interesting native substrate NATEE was also investigated and formation of the corresponding dopaquinone could be observed with a TON of 18 during the first 2 h of oxygenation. Finally, 4-methylphenol was subjected to catalytic oxygenation reactions whereby a competition reaction was observed, leading to a lower TOF than expected for this activated substrate.

In summary, we have investigated copper(I) complexes supported by bidentate bis(pyrazolyl)methane ligands as catalysts for the monooxygenation of a range of monophenolic substrates, closely mimicking the reactivity of the enzyme tyrosinase. Importantly, catalytic conversion to *ortho*-quinones was observed for all combinations of substrates and catalysts, thus enlarging the scope of biomimetic oxygenation reactions mediated by tyrosinase model systems. Of course, the unmatched activity of the enzyme still leaves room for further improvement of these artificial systems.

Supplementary material

Electronic Supplementary Information (ESI) available: [Materials and methods, ligand syntheses, complex syntheses, UV/vis measurements, NMR measurements].

Acknowledgments

The authors would like to thank Deutsche Forschungsgemeinschaft (DFG), CAU Kiel and COST CM 1003 for support of this research.

Disclosure statement

No potential conflict of interest was reported by the authors.

Funding

This work was supported by Deutsche Forschungsgemeinschaft [grant number Tu58/13].

References

- [1] M. Rolff, J. Schottenheim, H. Decker, F. Tuczek. *Chem. Soc. Rev.*, **40**, 4077 (2011).
- [2] E.I. Solomon, D.E. Heppner, E.M. Johnston, J.W. Ginsbach, J. Cirera, M. Qayyum, M.T. Kieber-Emmons, C.H. Kjaergaard, R.G. Hadt, L. Tian. *Chem. Rev.*, **114**, 3659 (2014).
- [3] Á. Sánchez-Ferrer, J.N. Rodríguez-López, F. García-Cánovas, F. García-Carmona. *Biochim. Biophys. Acta, Prot. Struct. Mol. Enzym.* **1247**, 1 (1995).
- [4] K.E. van Holde, K.I. Miller, H. Decker. *J. Biol. Chem.*, **276**, 15563 (2001).
- [5] Y. Matoba, T. Kumagai, A. Yamamoto, H. Yoshitsu, M. Sugiyama. *J. Biol. Chem.*, **281**, 8981 (2006).
- [6] Y.C. Li, Y. Wang, H.B. Jiang, J.P. Deng. *Proc. Natl. Acad. Sci. USA*, **106**, 17002 (2009).
- [7] M. Sendovski, M. Kanteev, V.S. Ben-Yosef, N. Adir, A. Fishman. *J. Mol. Biol.*, **405**, 227 (2011).
- [8] W.T. Ismaya, H.J. Rozeboom, A. Weijn, J.J. Mes, F. Fusetti, H.J. Wichers, B.W. Dijkstra. *Biochemistry*, **50**, 5477 (2011).
- [9] H. Decker, T. Schweikardt, F. Tuczek. *Angew. Chem. Int. Ed.*, **45**, 4546 (2006).
- [10] K. Selmečzi, M. Réglér, G. Michel, G. Speier. *Coord. Chem. Rev.*, **245**, 191 (2003).

- [11] K.D. Karlin, S. Kaderli, A.D. Zuberbühler. *Acc. Chem. Res.*, **30**, 139 (1997).
- [12] M. Rolff, J.N. Hamann, F. Tuczek. *Angew. Chem. Int. Ed.*, **50**, 6924 (2011).
- [13] E.A. Lewis, W.B. Tolman. *Chem. Rev.*, **104**, 1047 (2004).
- [14] L.M. Mirica, X. Ottenwaelde, T.D.P. Stack. *Chem. Rev.*, **104**, 1013 (2004).
- [15] A. De, S. Mandal, R. Mukherjee. *J. Inorg. Biochem.*, **102**, 1170 (2008).
- [16] K.D. Karlin, J.C. Hayes, Y. Gultneh, R.W. Cruse, J.W. McKown, J.P. Hutchinson, J. Zubieta. *J. Am. Chem. Soc.*, **106**, 2121 (1984).
- [17] J.N. Hamann, M. Rolff, F. Tuczek. *Dalton Trans.*, **44**, 3251 (2015).
- [18] L. Casella, M. Gullotti, M. Bartosek, G. Pallanza, E. Laurenti. *J. Chem. Soc., Chem. Commun.*, **18**, 1235 (1991).
- [19] M. Réglie, C. Jorand, B. Waegell. *J. Chem. Soc., Chem. Commun.*, **24**, 1752 (1990).
- [20] M. Rolff, J. Schottenheim, G. Peters, F. Tuczek. *Angew. Chem. Int. Ed.*, **49**, 6438 (2010).
- [21] L.M. Mirica, M. Vance, D.J. Rudd, B. Hedman, K.O. Hodgson, E.I. Solomon, T.D.P. Stack. *Science*, **308**, 1890 (2005).
- [22] A. Hoffmann, C. Citek, S. Binder, A. Goos, M. Rübhausen, O. Troeppner, I. Ivanović-Burmazović, E.C. Wasinger, T.D.P. Stack, S. Herres-Pawlis. *Angew. Chem. Int. Ed.*, **52**, 5398 (2013).
- [23] J.N. Hamann, F. Tuczek. *Chem. Commun.*, **50**, 2298 (2014).
- [24] J. Schottenheim, N. Fateeva, W. Thimm, J. Krahmer, F. Tuczek. *Z. Anorg. Allg. Chem.*, **639**, 1491 (2013).
- [25] J. Schottenheim, C. Gernert, B. Herzigkeit, J. Krahmer, F. Tuczek. *Eur. J. Inorg. Chem.*, **21**, 3501 (2015). doi:10.1002/ejic.201500029.
- [26] C. Wilfer, P. Liebhäuser, H. Erdmann, A. Hoffmann, S. Herres-Pawlis. *Eur. J. Inorg. Chem.*, **3**, 494 (2015).
- [27] A.S. Potapov, A.I. Khlebnikov. *Polyhedron*, **25**, 2683 (2006).
- [28] W. Flaig, Th. Ploetz, A. Küllmer. *Z. Naturforsch.*, **10b**, 668 (1955).
- [29] S.I. Bailey, I.M. Ritchie, Z. Hong-Guang. *Bioelectrochem. Bioenerg.*, **19**, 521 (1988).
- [30] V. Kahn, N. Ben-Shalom. *Pigm. Cell Res.*, **11**, 24 (1998).
- [31] J.H. Waite. *Anal. Biochem.*, **75**, 211 (1976).
- [32] E.I. Solomon, F. Tuczek, D.E. Root, C.A. Brown. *Chem. Rev.*, **94**, 827 (1994).
- [33] S.W. Taylor, T.F. Molinski, L.M. Rzepecki, J.H. Waite. *J. Nat. Prod.*, **54**, 918 (1991).
- [34] M.J. Nilges, H.M. Swartz, P.A. Riley. *J. Biol. Chem.*, **259**, 2446 (1984).
- [35] S.V. Jovanovic, K. Kónya, J.C. Scaiano. *Can. J. Chem.*, **73**, 1803 (1995).
- [36] W.K. Seok, T.J. Meyer. *J. Am. Chem. Soc.*, **110**, 7358 (1988).
- [37] P. Verma, J. Weir, L. Mirica, T.D.P. Stack. *Inorg. Chem.*, **50**, 9816 (2011).